Published in: *ASCE Journal of Structural Engineering*, 138(7), 922-931.
DOI: http://dx.doi.org/10.1061/(ASCE)ST.1943-541X.0000530

The structural behavior of thin-walled metal silos subject to different flow channel sizes under eccentric discharge pressures

Adam J. Sadowski[1] and J. Michael Rotter F.ASCE[2]

Abstract

The condition of eccentric discharge is known to be one of the most critical for the design of thin-walled cylindrical metal silos. Significant progress has been made in recent years in devising a relatively realistic set of representative pressures for this load case. However, the consequences these may have on the predicted structural behavior of a silo are not yet fully understood.

This paper presents a detailed parametric study into the behavior of a custom-designed slender silo under a set of unsymmetrical pressures describing the action of an eccentric parallel-sided pipe flow channel of varying cross-sectional area. The results are compared with the reference axisymmetric case of concentric discharge. It is found that the predicted behavior is very complex indeed, and that geometric nonlinearity is of much greater significance for cylindrical shells under unsymmetrical load patterns than under symmetrical patterns. Further, it is found that eigenmode-affine imperfections, very deleterious under axisymmetric loading patters, are instead beneficial to the buckling strength of a silo under eccentric discharge, thus making them unsuitable for use in design for this load condition.

Affiliations

[1] Research Associate, The University of Edinburgh, Scotland, UK

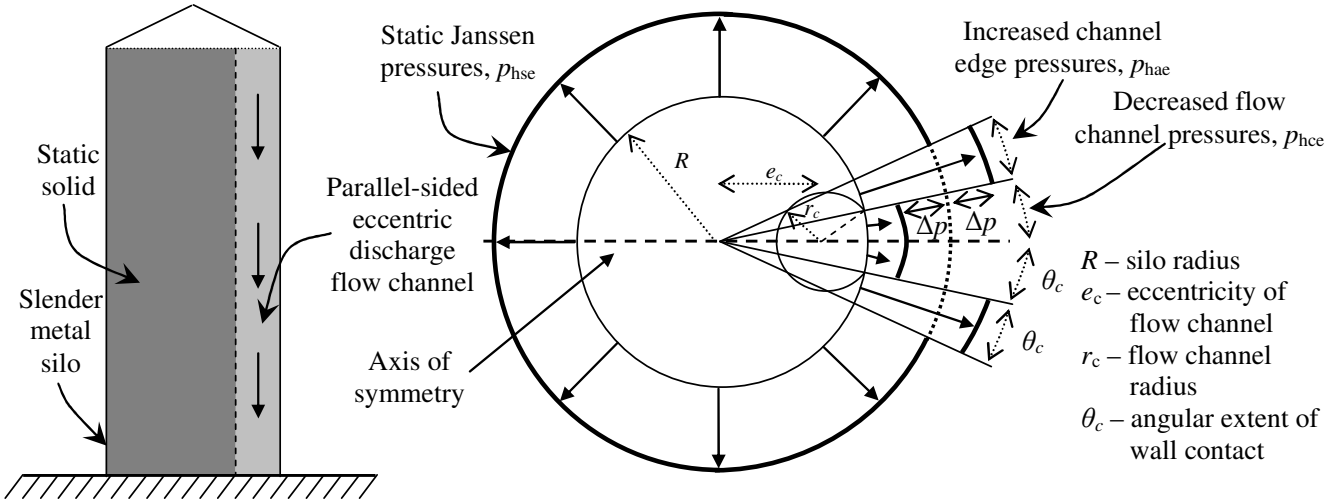
[2] Professor of Civil Engineering, The University of Edinburgh, Scotland, UK

Published in: *ASCE Journal of Structural Engineering*, 138(7), 922-931.
DOI: http://dx.doi.org/10.1061/(ASCE)ST.1943-541X.0000530

Introduction

Engineering background

Eccentric discharge is well known to be possibly the most serious design condition for cylindrical metal silos, a reputation well founded in the many catastrophic buckling failures for which it has been directly responsible. The difficulty in producing an appropriate yet accessible design criterion for this condition is compounded with the complexity of the mechanics and physics involved (Rotter, 2001) and the considerable practical challenges faced when carrying out experimental studies of eccentric discharge (Ooi *et al.*, 1990; Nielsen, 1998; Chen *et al.*, 2007).



a) Parallel-sided eccentric pipe flow channel

b) Geometry and notation of the EN 1991-4 (2006) eccentric discharge pressure model

Fig. 1 – Modelling of eccentric discharge in slender silos

In a significant development, Rotter (1986) applied a slice equilibrium analysis to a circular cross-section silo with a parallel-sided eccentric pipe flow channel (Fig. 1) to derive a reasonably realistic set of eccentric discharge pressures. This pressure model predicts a low normal pressure adjacent to the flow channel, slightly increased normal pressure near the sides and static near-Janssen normal pressure elsewhere; a simplification of what has been observed in experiments (e.g. Jenike, 1967; Hampe, 1987; Chen, 1996). The model has since been adopted in simplified form into the EN 1991-4 (2006) European Standard on Actions on Silos and Tanks (Fig. 1b).

Previous studies by the authors (Sadowski & Rotter, 2010; 2011a,b,c) addressed different aspects of the EN 1991-4 pressure model and its effects on the structural

Published in: *ASCE Journal of Structural Engineering*, 138(7), 922-931.
DOI: http://dx.doi.org/10.1061/(ASCE)ST.1943-541X.0000530

behavior and design requirements for thin-walled metal silos. Most importantly, these studies showed consistently that the main catalyst for failure under eccentric discharge is elastic buckling under axial compression, rather than material yielding under circumferential bending as suggested by Jenike (1967), Roberts and Ooms (1983) and others.

Variation of pressures with flow channel size in an eccentric discharge model

The size of the flow channel in an eccentric discharge pressure model of the type derived by Rotter (1986) and implemented in EN 1991-4 (2006) is most conveniently defined as the ratio of the flow channel radius to the silo radius, $\rho = r_c/R$, with both $\rho = 0.0$ and 1.0 being equivalent to concentric mass flow. The relative flow channel size is directly related to the channel wall contact angle θ_c (Fig. 1b) which is obtained from geometrical relations.

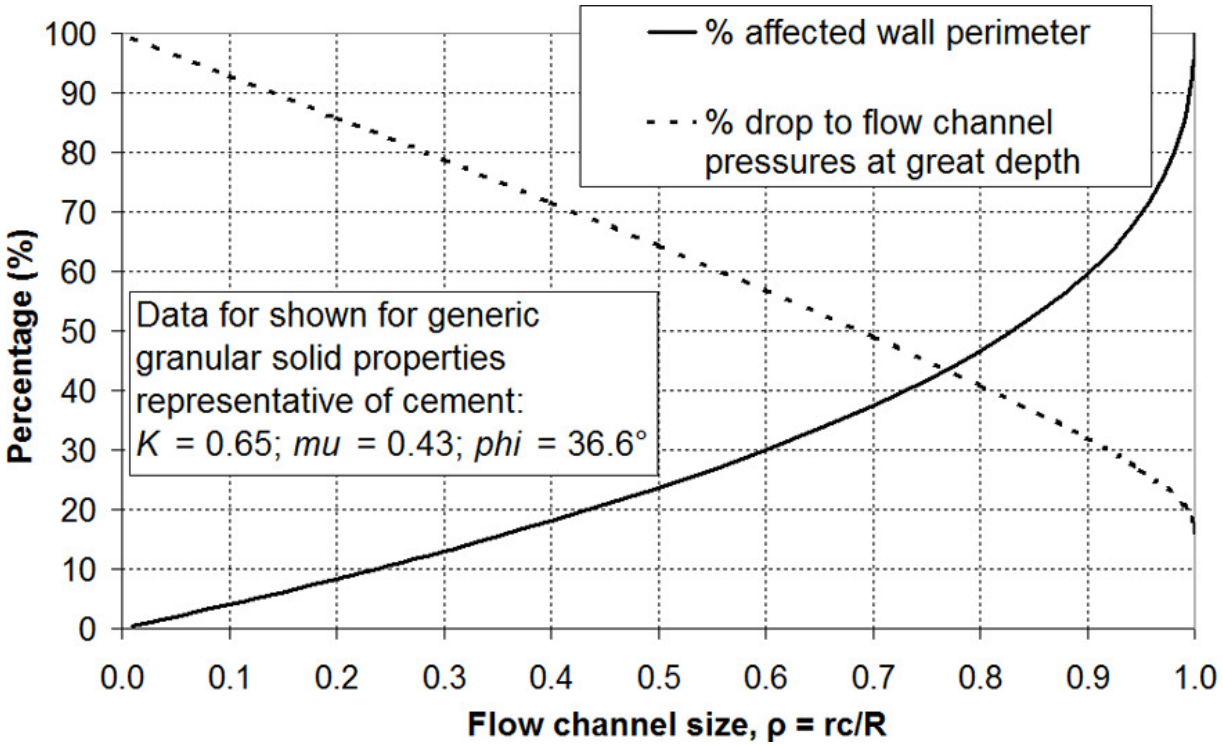


Fig. 2 – Variation of the wall contact parameter and flow channel percentage pressure drop with relative flow channel size ρ

In the EN 1991-4 version, for example, the combined region of decreased and increased pressures associated with the flow channel and its adjacent effects is prescribed to cover a circumferential spread of $2\theta_c$ around half of the silo wall. The

Published in: *ASCE Journal of Structural Engineering*, 138(7), 922-931.
DOI: http://dx.doi.org/10.1061/(ASCE)ST.1943-541X.0000530

relationship between the perimeter cover of flow channel pressures, $2\theta_c/\pi$, and the relative flow channel size ρ is close to linear (Fig. 2) until approximately ρ = 0.7, after which the perimeter cover rises rapidly for only small increases in ρ. For very small channels that are in contact with only a small portion of the silo wall, the EN 1991-4 model predicts a large drop in wall pressure at the centre of the channel. Further, this model also predicts a rise in wall pressure at the edges of the channel equal to the drop at the centre. Combined, this leads to an unduly severe loading on the silo for small channels, ρ ≤ 0.2 (Fig. 3a). Such channels do often arise in the form of a rathole in a funnel flow silo containing cohesive solids (Rotter, 2001), in which case the solid in the flow channel would have discharged completely leaving an empty hole with *zero* normal pressure running throughout the full silo height. Conversely, wall pressures in larger flow channels approach the stationary Janssen values corresponding to those for the wall friction and lateral pressure ratio. A very large channel with ρ > 0.7 (Fig. 3b) thus sees only very thin zones of static solid exerting a higher pressure on the wall over the entire height of the silo.

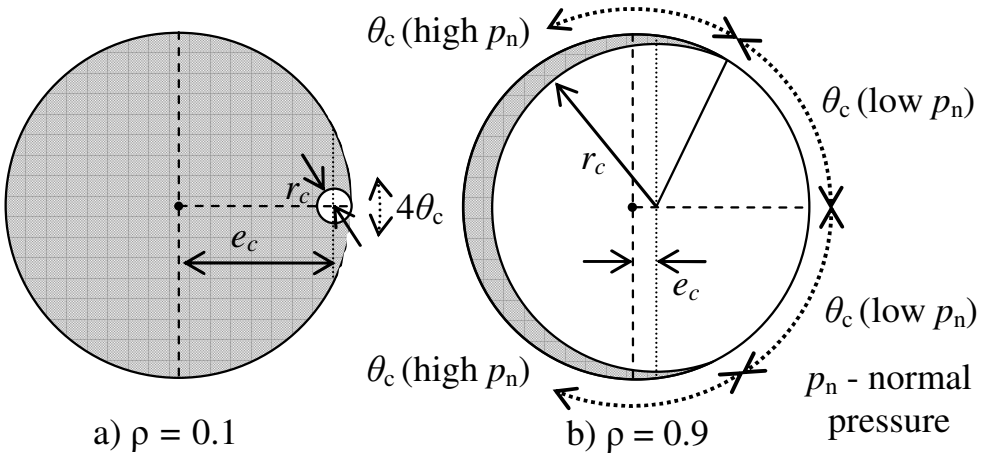


Fig. 3 – Very small and very large flow channel geometries according to EN 1991-4

The above version of the eccentric discharge flow model is therefore somewhat conceptually uncertain at both very small and very large values of the relative flow channel size ρ. Since the model was not devised with such conditions in mind, the predictions of this model should be treated with care for extreme values of ρ. However, since only ρ = 0.25, 0.4 and 0.6 are notionally recommended by EN 1991-

Published in: *ASCE Journal of Structural Engineering*, 138(7), 922-931.
DOI: http://dx.doi.org/10.1061/(ASCE)ST.1943-541X.0000530

4, the official design procedure should be shielded from these extreme values unless a National Annex requires otherwise.

Investigation of eigenmode-affine imperfections under eccentric discharge

According to the rules of the European Standard on the Strength and Stability of Shell Structures EN 1993-1-6 (2007), an analyst undertaking a full geometrically and materially nonlinear structural analysis with explicit modelling of imperfections (GMNIA) is required to find the most deleterious imperfection form. Traditionally, and in common with the treatment of beams and columns, this has been taken to be the first linear buckling eigenmode of the perfect shell (Koiter, 1945; 1963; Teng and Song, 2001; Rotter 2004) or alternatively the shape of the shell after buckling found in an elastic nonlinear analysis (Esslinger and Geier, 1972; Yamaki, 1984; Guggenberger *et al.*, 2004). The analyst is free to choose a different imperfection form if it can be justified, such as the axisymmetric weld imperfection of Rotter and Teng (1989) which has a practical basis and is widely considered as possibly the most damaging imperfection form for axial compression under axisymmetric loading (e.g. Knödel *et al.*, 1995; Rotter, 2004; Song *et al.*, 2004). However, recent studies of the axisymmetric weld depression (Sadowski & Rotter, 2011c) have revealed that this is not a very deleterious imperfection form under eccentric discharge due to the stiffening effect of the weld depression when the silo wall is subject to circumferential bending. Thus, a satisfactory imperfection form for eccentric discharge still remains to be found.

Objectives of the present paper

This paper presents a detailed parametric study into the structural effects of incremental changes in the radius of the flow channel under eccentric pipe flow discharge (Fig. 1). The flow channel size was again defined as the ratio of the flow channel and silo radii, $\rho = r_c/R$, and was varied from $\rho = 0.0$ to 0.9 at intervals of 0.1. One goal of this study is to determine whether the 'default' values of $\rho = 0.25$, 0.4 and 0.6, as recommended by EN 1991-4, are a satisfactory and sufficiently conservative choice for structural design. This parametric study is undertaken through a series of linear and nonlinear shell buckling computations, as defined by EN 1993-1-6, performed with the ABAQUS (2009) finite element software on an example silo. These include a linear-elastic reference stress analysis (LA), linear bifurcation

Published in: *ASCE Journal of Structural Engineering*, 138(7), 922-931.
DOI: http://dx.doi.org/10.1061/(ASCE)ST.1943-541X.0000530

analysis (LBA) to obtain the first linear buckling eigenmode and load factor, a geometrically linear and materially nonlinear analysis (MNA) to obtain the load factor at plastic collapse, a geometrically nonlinear elastic analysis (GNA) to obtain the incremental buckling mode, load factor and nonlinear stresses at buckling, and finally the same but with explicit modelling of material nonlinearity (GMNA).

This paper additionally explores whether an 'eigenmode-affine' imperfection form does indeed result in a decrease in the predicted buckling strength under this eccentric discharge pressure pattern. The imperfection forms investigated include: a) the inward 1st LBA mode with shape deviations unfavourably oriented towards the centre of the shell; b) the outward 1st LBA mode with shape deviations in the reversed direction; and c) the deformed shape at the instant before buckling in a geometrically nonlinear analysis (GNA) to assess the effect of pre-buckling deformations.

Design and modelling of an example silo

A very slender, flat-bottomed, cylindrical silo with a height of 26 m and radius of 2.5 m (aspect ratio H/D = 5.2) was designed according to the structural hand-design procedure of EN 1993-1-6 (2007) and EN 1993-4-1 (2007). The design loading consisted of the normal pressures and frictional tractions arising from concentric discharge of 510 m^3 of a generic granular material with properties similar to those of cement. The properties for cement were taken from EN 1991-4 (2006) Annex E for the maximum friction load case and a D2 'smooth' wall. These may be considered as representative of a wide range of granular materials because over 70% of the materials listed in that Annex have properties within one standard deviation of the mean values for cement. Action Assessment Class 2 was assumed based on the storage capacity. The values of the respective discharge factors for normal pressures (C_h) and frictional tractions (C_w) were taken as 1.15 and 1.1. The overall partial safety factor is 1.65 according to EN 1993-4-1.

The silo wall was assumed to be of isotropic mild steel with elastic modulus E = 200 GPa, Poisson's ratio ν = 0.3 and yield stress σ_y = 250 MPa (ideal elastic-plastic). The wall was designed to vary in a stepwise manner from a thickness of 3 mm at the top to 9 mm at the outlet so that the base of each wall strake was critical for buckling under

Published in: *ASCE Journal of Structural Engineering*, 138(7), 922-931.
DOI: http://dx.doi.org/10.1061/(ASCE)ST.1943-541X.0000530

concentric discharge pressures only (Fig 4). The beneficial effect of axisymmetric internal pressure was included in the buckling strength assessment. The Fabrication Tolerance Quality Class was taken to be C or 'Normal', requiring deeper imperfections to be used in both design and subsequent numerical modelling.

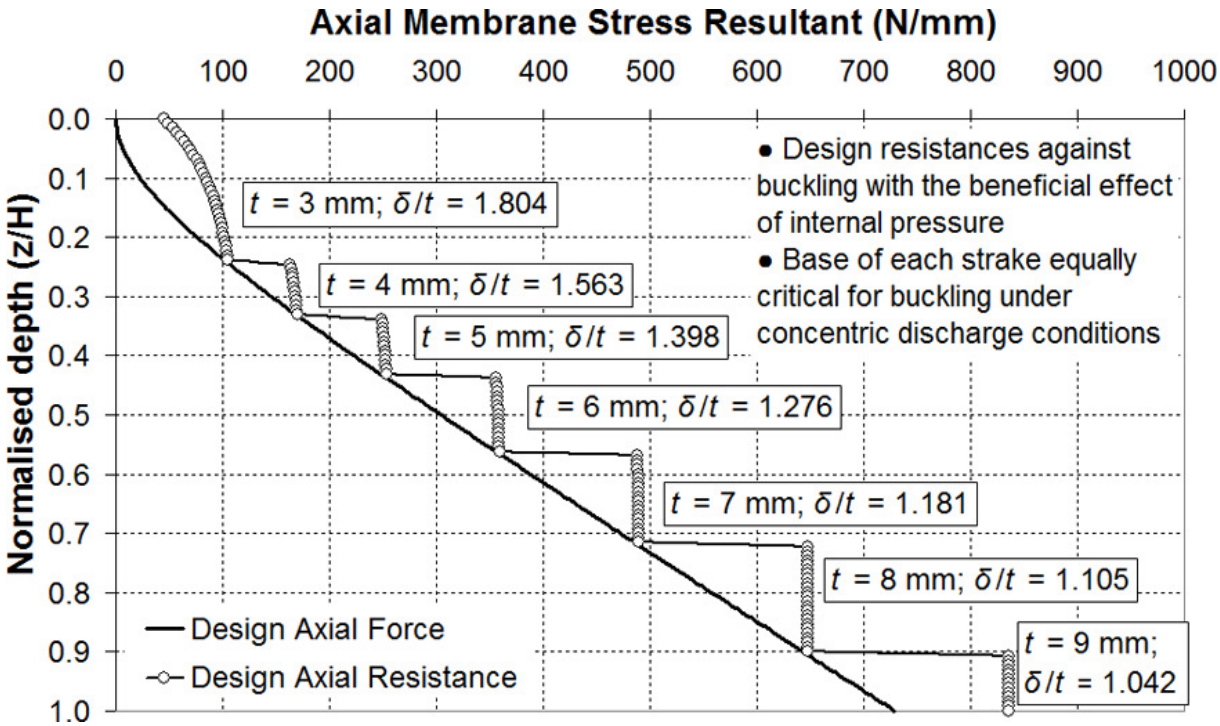


Fig. 4 – Meridional distribution of design axial force, design axial resistance, design wall thicknesses and local imperfection amplitudes

Further details of the design are not crucial to the understanding of the material presented in this paper. The interested reader may look elsewhere (e.g. Sadowski & Rotter, 2011a) to obtain full details of the silo design process used. Lastly, it should be noted that the application of eccentric discharge pressures to a silo that was clearly not designed to resist them reflects the current unfortunate state of affairs in this field and the high failure rate of silos under this loading condition.

The silo was modelled in ABAQUS (2009) using nine-node reduced integration S9R5 shell elements. The base of the silo wall was assumed to have a pinned boundary condition and only half of the silo wall was modelled using appropriate conditions of symmetry (Fig. 1b) to economise on elements and computation time. Further, the silo cylinder was modelled as being connected to a conical roof with an inclination of 15°

Published in: *ASCE Journal of Structural Engineering*, 138(7), 922-931.
DOI: http://dx.doi.org/10.1061/(ASCE)ST.1943-541X.0000530

to the horizontal which restricts out-of-round displacements on the upper boundary in a more convincing way than a rigid body constraint. Such displacements are known to adversely affect the stress patterns in shells under unsymmetrical loads (Calladine, 1983).

Behavior of the perfect silo under eccentric pipe flow

Previous findings

Previous computational studies of the structural consequences of this formulation of eccentric pipe flow discharge (Rotter, 1986; Sadowski & Rotter, 2010; 2011a,b,c) explored the characteristic patterns of axial membrane stresses that develop under this condition and identified two critical locations for buckling failure (Fig. 5). The first location is across the flow channel at approximately midheight, where high compressive axial membrane stresses cause predominantly elastic local buckling. The wall stresses adjacent to the flow channel become tensile towards the bottom of the silo. The second location is at the base of the silo adjacent to the edge of the channel, where very high axial compression may result in predominantly plastic local buckling. Conversely, the channel edge stresses become tensile towards midheight.

Published in: *ASCE Journal of Structural Engineering*, 138(7), 922-931.
DOI: http://dx.doi.org/10.1061/(ASCE)ST.1943-541X.0000530

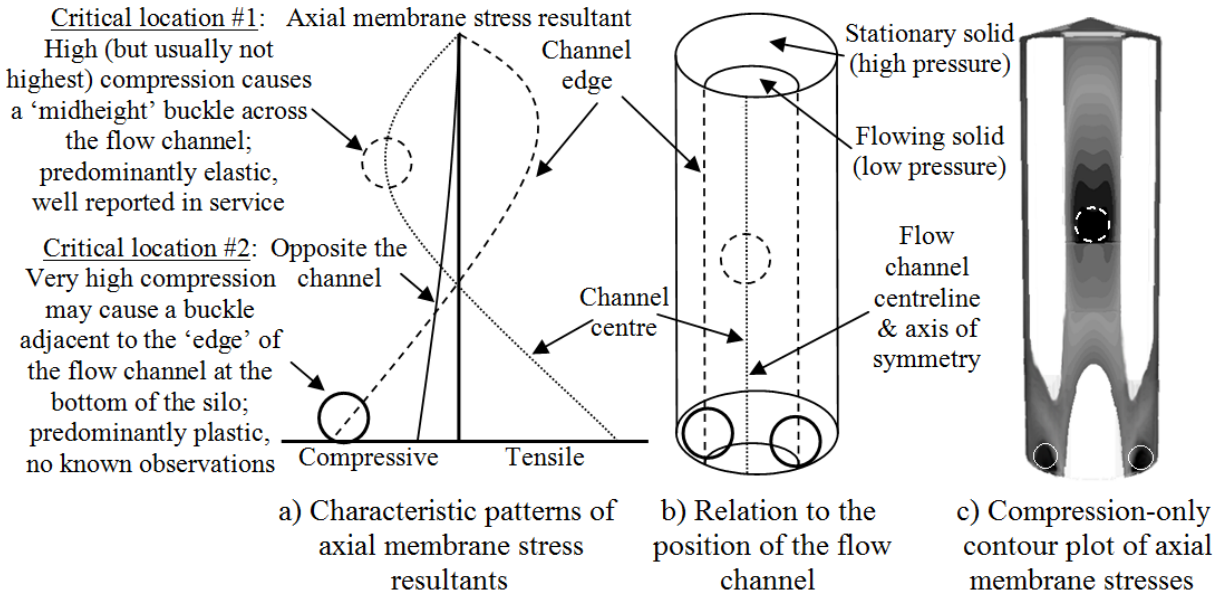


Fig. 5 – Illustration of characteristic axial membrane stress resultant patterns and possible critical buckling locations under eccentric pipe flow in silos, after Sadowski & Rotter (2011c)

This paper explores the effects of such eccentric discharge on a stepped wall thickness silo with a very slender aspect ratio (H/D = 5.2). As shown by Sadowski & Rotter (2011c), it is very likely that a perfect slender silo will exclusively exhibit the predominantly elastic 'midheight' buckling mode. This is due to the fact that the buckling resistance of a realistic stepped-wall thickness silo is significantly lower at midheight than at the base. Furthermore, the static solid near the base of the silo is known to offer a significant additional stiff restraint against buckling (Rotter & Zhang, 1990; Knödel *et al.*, 1995) which enhances the local buckling strength and prevents the buckle from forming at this location. The results presented in this paper suggest that the 'midheight' buckling mode is consistently critical for slender silos under the full possible range of flow channel sizes under eccentric pipe flow discharge.

Local meridional distributions of axial membrane stress resultants

The meridional distributions of axial membrane stress resultants in the silo wall across the flow channel for linear elastic (LA) analyses at the 1st linear buckling eigenvalue (LBA) and for the geometrically nonlinear analyses (GNA) at the instant before

Published in: *ASCE Journal of Structural Engineering*, 138(7), 922-931.
DOI: http://dx.doi.org/10.1061/(ASCE)ST.1943-541X.0000530

buckling are shown in Figs 6 and 7 respectively. It is clear from these that the emergence of the characteristic pattern of axial membrane stresses for eccentric pipe flow illustrated in Fig. 5a develops progressively as the relative flow channel size ρ increases, and really only appears for $\rho \geq 0.4$. Specifically, there is a clear development of a high compressive peak at approximately midheight.

For the LA axial membrane stresses at LBA buckling adjacent to the channel centre (Fig. 6), the compressive 'midheight' peak and tensile stresses near the base are present already under the action of the smallest flow channel size with $\rho = 0.1$. This compressive peak remains very high near the bottom of the 3 mm strake until $\rho = 0.5$, after which it gradually descends to approximately $z/H = 0.45$ for larger flow channels. The critical location for buckling, however, is always at the bottom of the 3 mm strake because the buckling resistance is lowest in this part of the wall. It is remarkable to note how unusually sensitive the axial membrane stress resultant is to step changes in local wall thicknesses for $\rho = 0.1$ and 0.2.

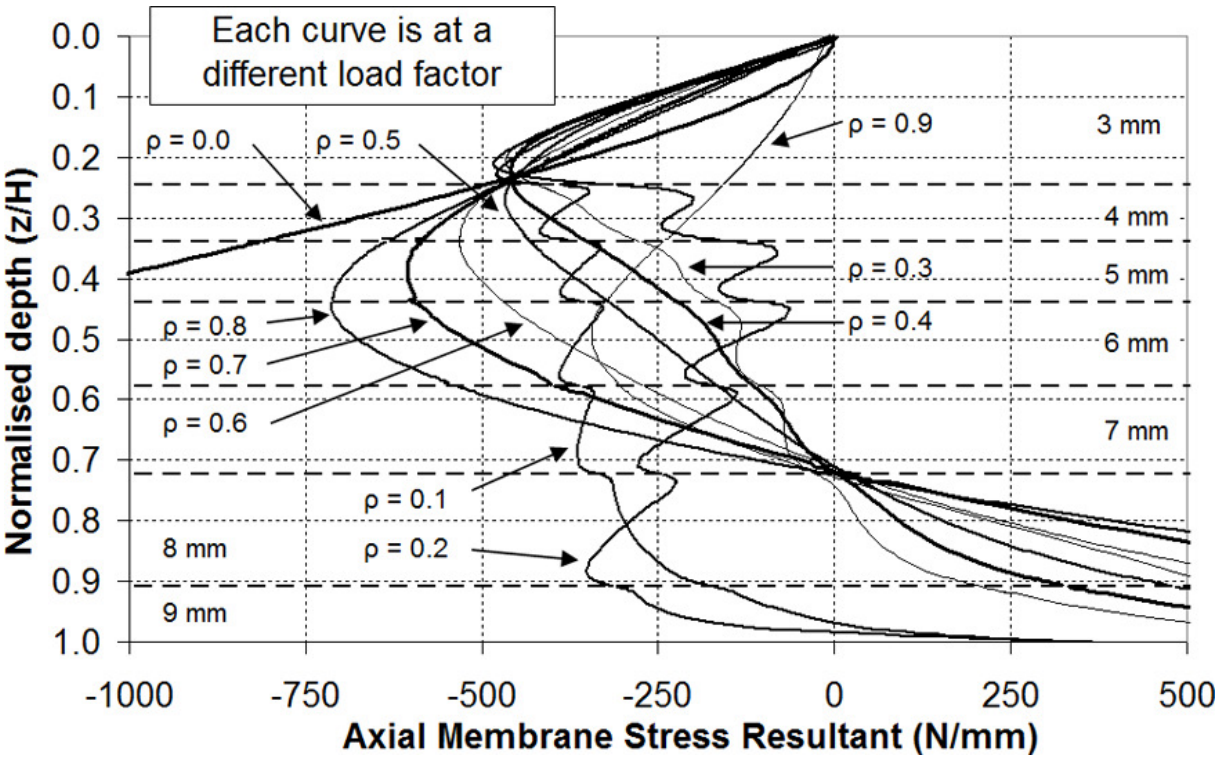


Fig. 6 – Meridional distributions of LA axial membrane stress resultants at buckling through channel centre (all at different load levels)

Published in: *ASCE Journal of Structural Engineering*, 138(7), 922-931.
DOI: http://dx.doi.org/10.1061/(ASCE)ST.1943-541X.0000530

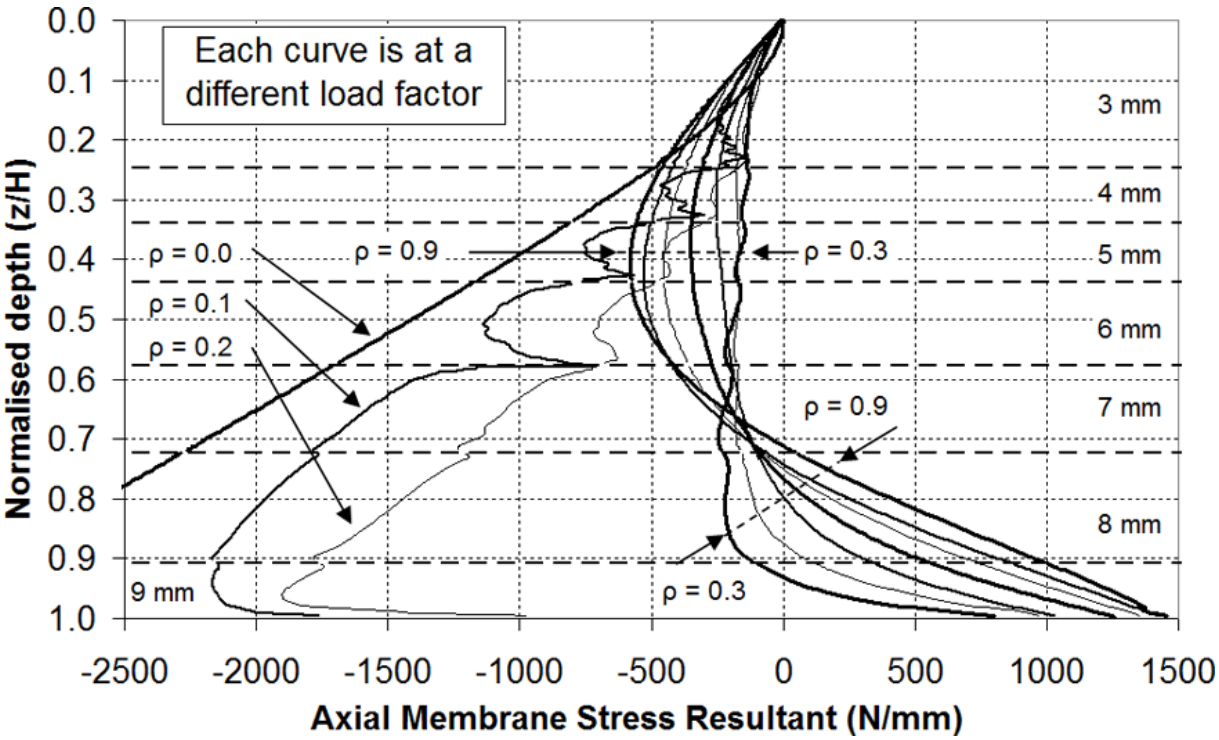


Fig. 7 – Meridional distribution of GNA buckling axial membrane stress resultants at buckling through channel centre (all at different load levels)

The nonlinear axial membrane stress resultant distributions (Fig. 7) show that the change from compressive to tensile at the base of the silo does not occur for the smallest channels in the range $0.0 \leq \rho \leq 0.1$, but for quite larger ones with $0.2 \leq \rho \leq 0.3$. Indeed, the curves for $\rho = 0.0$, 0.1 and 0.2 are clearly related, and illustrate the progressive local change in the stress pattern under the action of an increasingly wide region of low normal pressure. Further, where a linear analysis predicts a compressive peak at approximately midheight already for $\rho = 0.1$, this is not seen in a nonlinear analysis until the flow channel becomes as large as $\rho = 0.5$.

Global patterns of linear and nonlinear axial membrane stresses and buckling modes of the perfect silo

A more complete picture of the behavior of the perfect silo is presented next with the aid of a set of 3D contour plots of the LA (Fig. 8) and GNA (Fig. 9) compressive-only axial membrane stresses at the respective buckling load factors for each value of the relative flow channel size, $0.0 \leq \rho \leq 0.9$. These illustrate the progressive development of the pattern of axial membrane stresses that is characteristic of eccentric pipe flow (Fig. 5), and of the significant differences between the numerical predictions by the

Published in: *ASCE Journal of Structural Engineering*, 138(7), 922-931.
DOI: http://dx.doi.org/10.1061/(ASCE)ST.1943-541X.0000530

two types of analyses, especially for smaller channels. Note that Figs 8 and 9 have been digitally enhanced to darken the regions of highest axial compression and to make all regions in tension solid white, since tensile stresses are usually not of interest in a buckling analysis.

At $\rho = 0.0$ the silo is under concentric discharge: the axisymmetric axial compression increases monotonically towards the base of the silo, as in Fig. 4. The critical location for buckling in this case is at the bottom of the 3 mm strake but could have been in many alternative places because the silo was designed to make the bottom of each strake equally critical under axisymmetric loading. Detailed studies of the silo under concentric discharge may be found in Sadowski & Rotter (2011b).

The numerical predictions of the effects of pipe flow eccentric discharge show that when the analysis includes geometric nonlinearity, a very small flow channel acts very much like a local perturbation of the axisymmetric pressures caused by concentric discharge (Fig. 9). The strip-like characteristic pattern of axial membrane stresses associated with eccentric pipe flow (Fig. 5c) does not develop until the flow channel radius reaches 30% of the silo radius: $\rho = 0.3$. For flow channels smaller than this, the global stress state is very similar to that under concentric discharge. By contrast, a linear analysis indicates that this characteristic pattern exists at $\rho = 0.1$ (Fig. 8).

Published in: *ASCE Journal of Structural Engineering*, 138(7), 922-931.
DOI: http://dx.doi.org/10.1061/(ASCE)ST.1943-541X.0000530

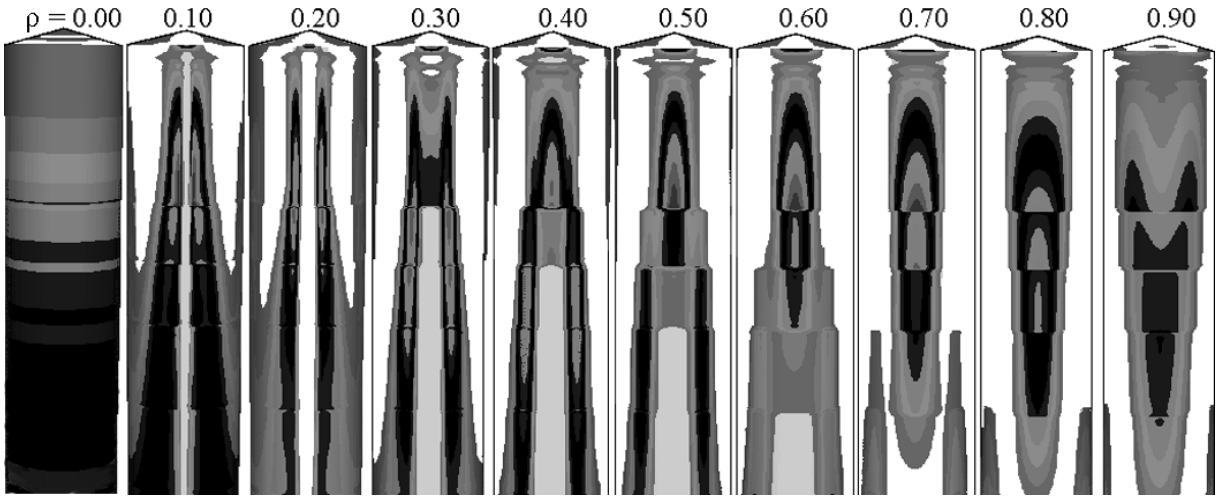


Fig. 8 – Contour plot of compressive-only LA axial membrane stresses at buckling (solid white regions show tension, darkest regions show highest compression)

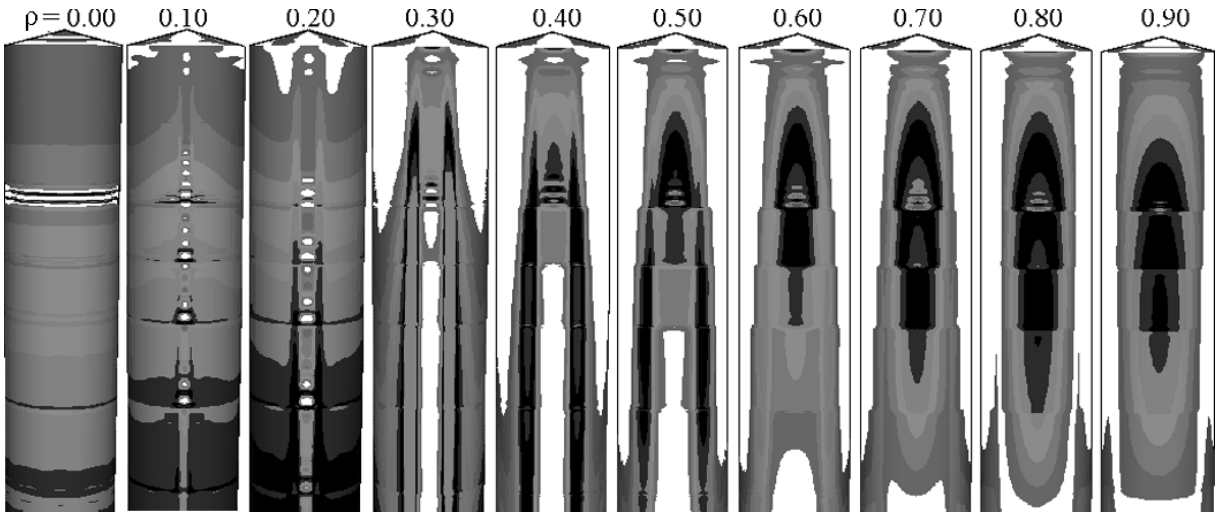


Fig. 9 – Contour plot of compressive-only GNA axial membrane stresses at buckling (solid white regions show tension, darkest regions show highest compression)

The linear bifurcation modes (LBA) and the GNA incremental buckling modes are shown in Figs 10 and 11 respectively. The LBA analyses consistently predict a localised elastic 'midheight' buckling mode for each of the flow channels with $\rho \geq 0.1$, directly reflecting the LA stress patterns shown in Figs 6 and 8. The nonlinear GNA analyses similarly predict the elastic 'midheight' buckling mode, but only for $\rho \geq 0.3$, which corresponds to the emergence of the characteristic strip-like global pattern of axial membrane stresses. The critical location is almost uniquely at the bottom of the thinnest and thus weakest 3 mm strake. For $\rho = 0.1$, the GNA buckling mode is actually predicted to occur on the opposite side of the silo to the side adjacent to the

Published in: *ASCE Journal of Structural Engineering*, 138(7), 922-931.
DOI: http://dx.doi.org/10.1061/(ASCE)ST.1943-541X.0000530

flow channel, and is thus not a 'midheight' buckle. Further, the mode for $\rho = 0.2$ exhibits several small buckles across the channel throughout the entire height of the silo. The global patterns of axial membrane stresses and buckling modes presented so far thus suggest that the range $0.0 < \rho < 0.3$ is a 'transitional' range in which the silo exhibits only a gradual shift in its nonlinear buckling behavior from that characteristic of concentric discharge to that characteristic of eccentric discharge.

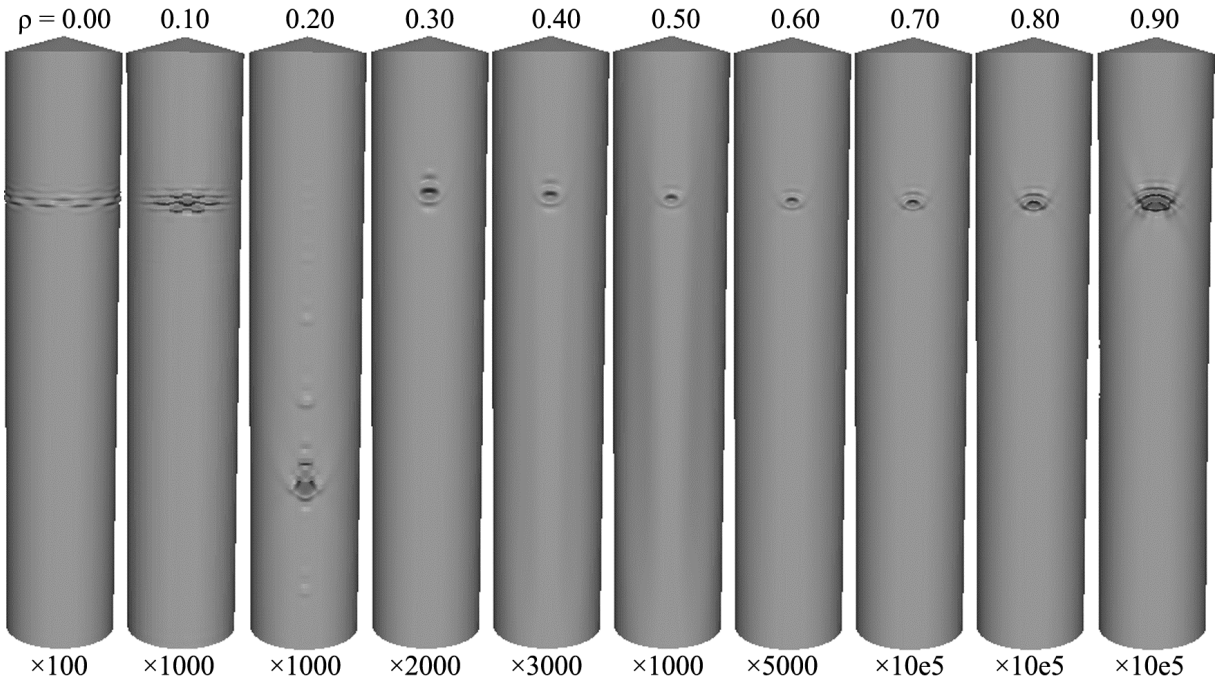


Fig. 10 – LBA linear bifurcation modes

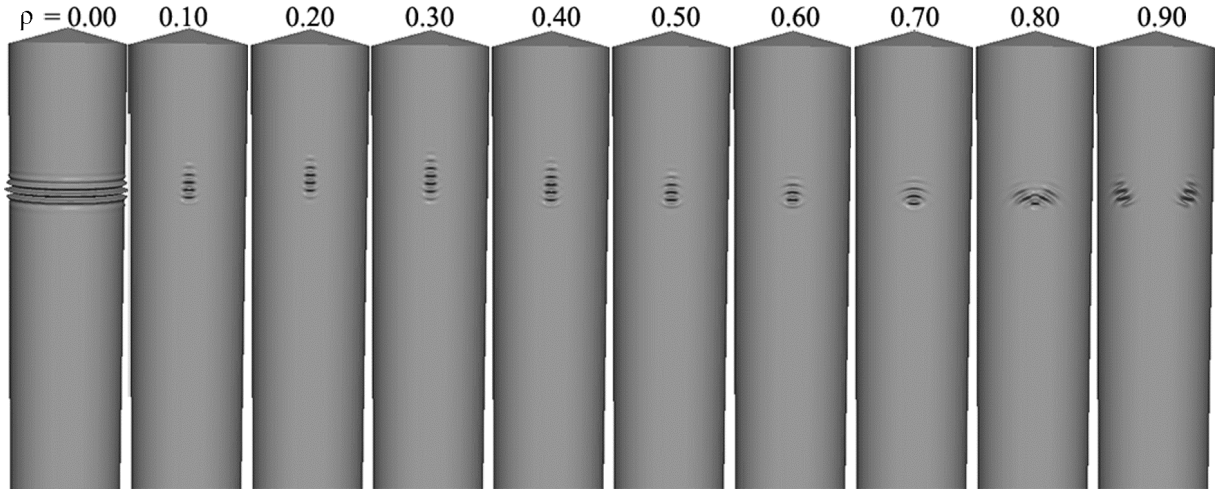


Fig. 11 – GNA incremental buckling modes

Published in: *ASCE Journal of Structural Engineering*, 138(7), 922-931.
DOI: http://dx.doi.org/10.1061/(ASCE)ST.1943-541X.0000530

Load proportionality factors for the perfect silo

The computed load factors for the perfect shell for each of the relative flow channel sizes are illustrated in Figs 12 and 13. Under concentric discharge ($\rho = 0.0$), the introduction of geometric and then material nonlinearity produces a progressive decrease in the predicted buckling strength: an outcome that is very typical of analyses of shells under axisymmetric loading. The behavior is especially sensitive to material plasticity, with the GMNA analysis predicting an elastic-plastic elephant's foot buckling mode (not shown).

Table 1 – Load factors for the perfect silo (values in **bold** represent a predicted elastic 'midheight' buckling mode, characteristic of eccentric pipe flow discharge)

$\rho = r_c/R$	0.00	0.10	0.20	0.25	0.30	0.40	0.50	0.60	0.70	0.80	0.90
LBA	7.65	**1.49**	**1.06**	**0.47**	**0.36**	**0.25**	**0.20**	**0.21**	**0.26**	**0.44**	**0.77**
MNA	4.54	2.51	1.14	0.88	0.77	0.64	0.60	0.65	0.75	0.94	1.52
GNA	7.63	6.77	4.51	**2.55**	**0.81**	**0.49**	**0.33**	**0.37**	**0.41**	**0.63**	**1.18**
GMNA	3.85	3.71	3.60	**2.55**	**0.81**	**0.49**	**0.33**	**0.37**	**0.41**	**0.63**	**1.18**
GNA/LBA	0.997	4.54	4.25	5.43	2.25	1.96	1.65	1.76	1.58	1.43	1.53
GNA/GMNA	1.98	1.82	1.25	1.00	1.00	1.00	1.00	1.00	1.00	1.00	1.00

The smallest channel size of $\rho = 0.1$, whose unsymmetrical pressure components cover barely 4% of the silo wall (Fig. 2), was found to have a very deleterious effect on the buckling strength according to an LBA analysis: there is a drop in load factor of 81% from 7.64 to 1.49. But rather unexpectedly, this effect was found to be much milder according to a GNA analysis (a drop of only 11% from 7.62 to 6.77) and even milder still according to a GMNA analysis (a drop of merely 3.6% from 3.85 to 3.71). This shows that geometric nonlinearity often has a very beneficial effect on the buckling strength under eccentric discharge. This beneficial effect becomes smaller in absolute terms as the flow channel size increases, but the GNA factor remains on average 75% higher than the LBA factor in the range $0.3 \leq \rho \leq 0.9$. Subsequent increases in flow channel size result in further decreases in the buckling strength until

Published in: *ASCE Journal of Structural Engineering*, 138(7), 922-931.
DOI: http://dx.doi.org/10.1061/(ASCE)ST.1943-541X.0000530

approximately ρ = 0.6, after which there is a mild recovery. This suggests that mid-sized flow channels are the most severe.

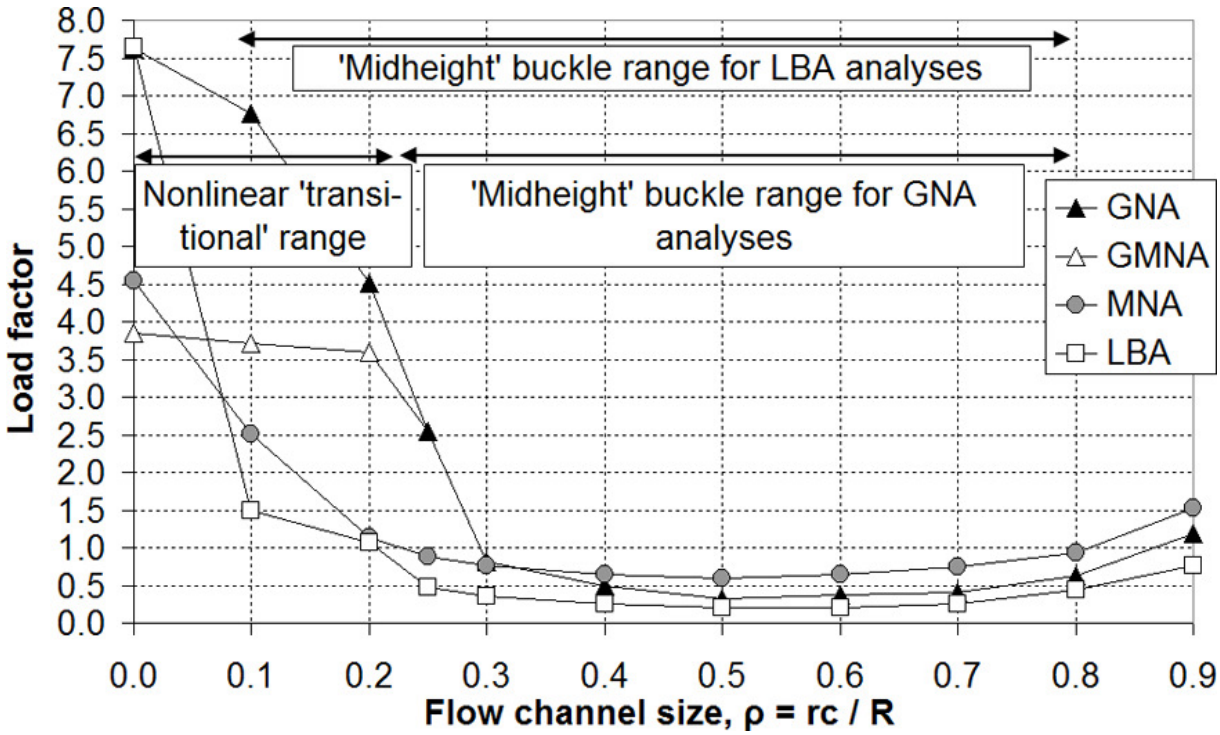


Fig. 12 – Variation of computed load factors for the perfect silo with the relative flow channel size; global view

Published in: *ASCE Journal of Structural Engineering*, 138(7), 922-931.
DOI: http://dx.doi.org/10.1061/(ASCE)ST.1943-541X.0000530

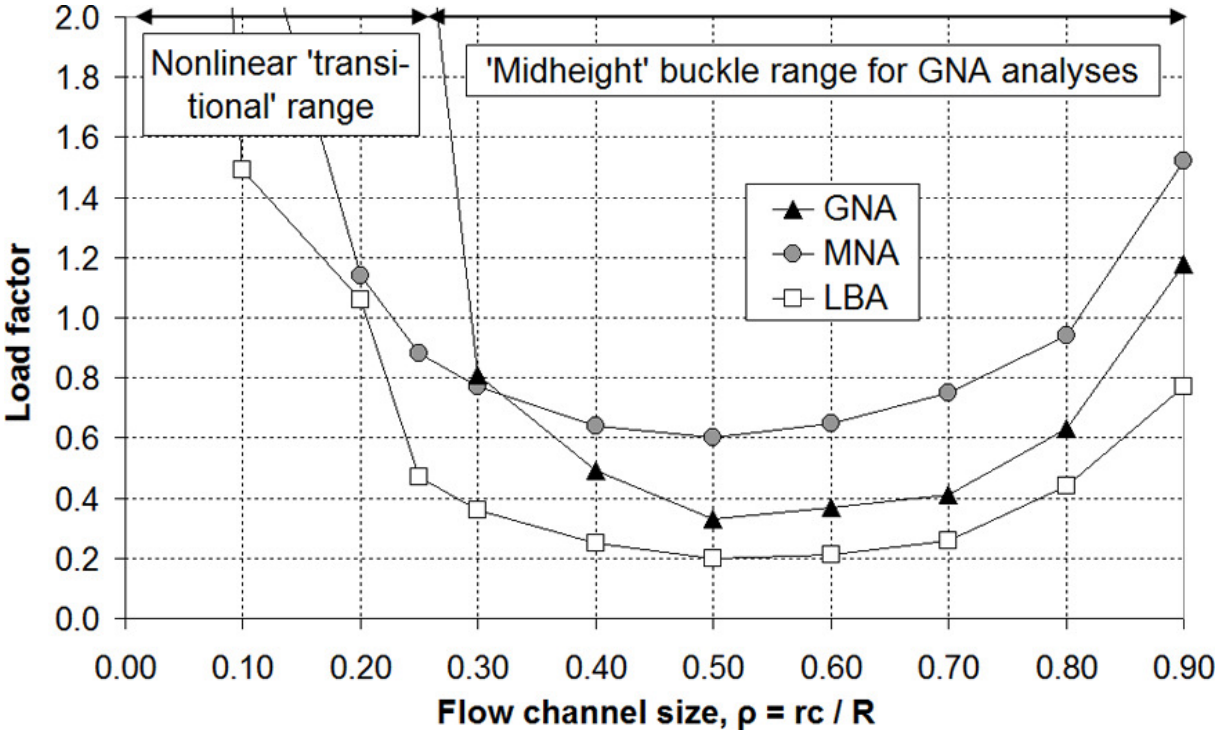


Fig. 13 – Variation of computed load factors for the perfect silo with the relative flow channel size; close-up of range with lowest load factors

Material plasticity plays no further role in the structural behavior of the silo beyond approximately $\rho = 0.25$. This is reflected in the *entirely* elastic response (GNA = GMNA) from this point on, and the fact that the MNA load factor is higher than all others. Thus the silo under eccentric pipe flow does *not* fail by plastic collapse due to high circumferential bending, despite assumptions made in earlier work that it may (e.g. Jenike (1967), Roberts and Ooms (1983), Bucklin *et al.*, (1990)). However, over the range of flow channels where the nonlinear behavior is still in transition from concentric to eccentric ($\rho \leq 0.2$), plasticity still significantly affects the buckling strength, always adversely.

In interpreting the above results for application in silo design, it is clear that the specified analysis should be devised to predict the strip-like global pattern of axial membrane stresses that is responsible for the elastic 'midheight' buckling mode (Figs 8 to 11). From Figs 12 and 13, it is clear that if this buckling mode is obtained, then the corresponding load factor is at or very close to the minimum of the load factor vs. channel size curve. A nonlinear analysis which instead predicts that the behavior of the silo is still in the 'transitional' range places the associated load factor quite far

away from this minimum. The key to this outcome from a buckling analysis lies in the load definition. Given the difficulty inherent in accurately predicting flow channel sizes, a prescription of flow channels that are mid-sized or larger in a codified standard may be necessary to ensure that only the most critical condition is considered, leading to a conservative design. The EN 1991-4 standard has attempted to produce such a load definition, but it is evident that its channel size definitions require some modification.

The uncertainty of this eccentric discharge pressure model near the two extremes of the range of possible channel sizes (Fig. 3) and the FE evidence presented so far both suggest that it would be wise to *revise* the values that are currently recommended in the EN 1991-4 standard (ρ = 0.25, 0.4 and 0.6). It is advised that the ranges should be limited to $0.2 \leq \rho \leq 0.7$ for linear analyses and $0.4 \leq \rho \leq 0.7$ for nonlinear analyses, since the characteristic pattern of eccentric discharge pressures requires larger flow channels to develop when geometric nonlinearity is included. If three suitable values of ρ are specifically required, these may perhaps be taken as 0.4, 0.55 and 0.7.

Exploration of the beneficial effect of geometric nonlinearity

This section considers only stresses extracted at the bottom of the thinnest 3 mm strake, which has been shown to be the consistently critical location for both concentric and eccentric discharge analyses for this example silo (Figs 10 and 11). The circumferential distributions of axial membrane stress resultants at this location for LA analyses at the LBA buckling factor and GNA analyses at buckling are shown in Figs 14 and 15 respectively. The common features shared by most of these curves include a region of high axial compression at the centre of the flow channel, followed a rapid change to high membrane tension, and leading to a subsequent decay to the reference axisymmetric compression value on the far side of the silo, opposite the flow channel. The gradual transition in characteristic stress patterns from concentric to eccentric discharge is best illustrated by the GNA stress curves at buckling for $0.0 \leq \rho \leq 0.3$ in Fig. 15. For ρ = 0.1 and 0.2, the stresses are still close to the reference axisymmetric value, though the local effect of the flow channel is clearly visible near $\theta = 0°$. The magnitude of the perturbed value of the membrane compression at

Published in: *ASCE Journal of Structural Engineering*, 138(7), 922-931.
DOI: http://dx.doi.org/10.1061/(ASCE)ST.1943-541X.0000530

buckling opposite the channel decreases together with ρ and the load factor, and eventually the channel becomes large enough (ρ ≥ 0.3) to induce membrane tension.

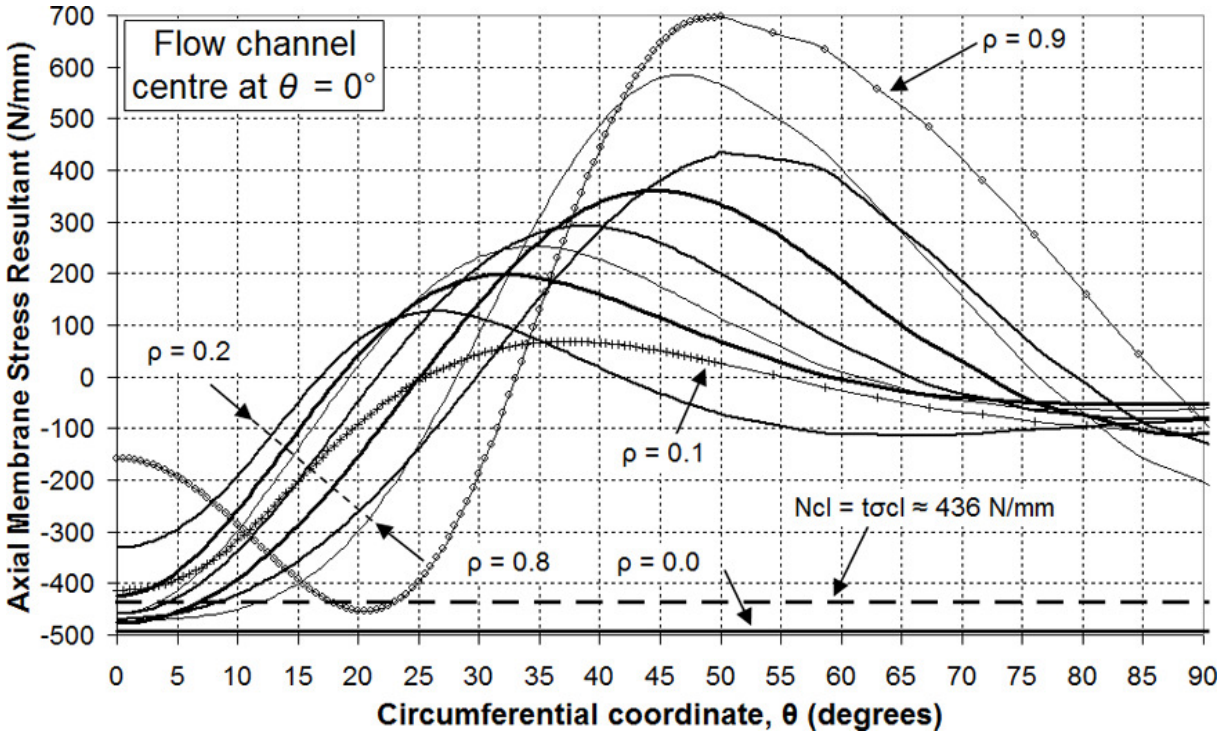


Fig. 14 – Circumferential distribution of LA axial membrane stress resultants at LBA buckling at the bottom of the 3 mm strake relative to the channel centre ($\theta = 0°$)

Published in: *ASCE Journal of Structural Engineering*, 138(7), 922-931.
DOI: http://dx.doi.org/10.1061/(ASCE)ST.1943-541X.0000530

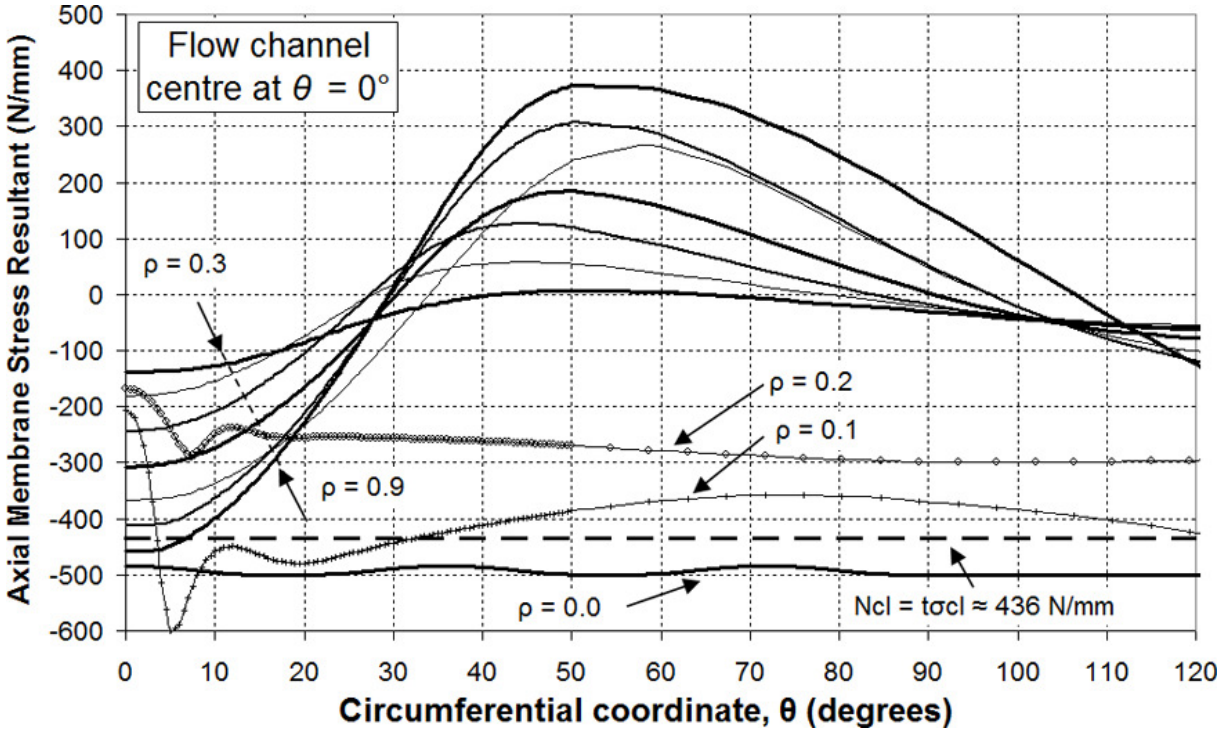


Fig. 15 – Circumferential distribution of GNA axial membrane stress resultants at buckling at the bottom of the 3 mm strake relative to the channel centre ($\theta = 0°$)

Where unsymmetrical distributions of axial compressive stresses occur such as those in Figs 14 and 15, the features that are of greatest interest in a buckling assessment are the angular extent to which the axial membrane stress resultants are compressive and what the peak compression is through the plane of symmetry (Fig. 16). These properties were thus extracted and are shown in Figs 17 and 18 for several values of the flow channel size. The general pattern is that the half-spread of the compressive region (Fig. 17) and the peak compression (Fig. 18) both increase steadily with flow channel size. However, the compressive stresses from a GNA analysis consistently cover a significantly wider spread of the silo wall than those from a LA analysis, and attain a much lower peak compression for any size of flow channel in the given range. A geometrically nonlinear analysis therefore reveals that the portion of the shell that is mobilised to resist the effects of the eccentric pipe flow channel is much greater than is expected by a linear analysis. This greater spread in turn results in a lower overall magnitude of compression and subsequently a higher buckling load. This beneficial effect is substantial, and may lead to increases in the load factor by as much as 75%.

Published in: *ASCE Journal of Structural Engineering*, 138(7), 922-931.
DOI: http://dx.doi.org/10.1061/(ASCE)ST.1943-541X.0000530

It may be noted that the peak axial compressive stress at linear bifurcation (LA @ LBA) is close to, but slightly above, the simple classical critical value ($N_{cl} = t\sigma_{cl} \approx 0.605Et^2R^{-1} \approx 436$ N/mm for the 3 mm strake). This matches findings of earlier studies (e.g. Libai and Durban, 1973; 1977; Cai, 2003). The reasons for this slight increase above this critical value are twofold. Firstly, the stress reported is the peak value, but the buckle has a finite size so the non-uniformity of the stresses leads to a slight rise (Rotter, 1986). Secondly, the material immediately adjacent to the buckle is at even lower stresses (Fig. 15) which provides significant elastic restraint rather than just simply-supported boundaries to the buckle. Under a geometrically nonlinear analysis (GNA), buckling occurs at peak values of stress that are much lower (Fig. 18), which arises because the local flattening of the shell produces a much higher local radius of curvature (Rotter, 1985). This was also shown in the study of Rotter *et al*. (2011).

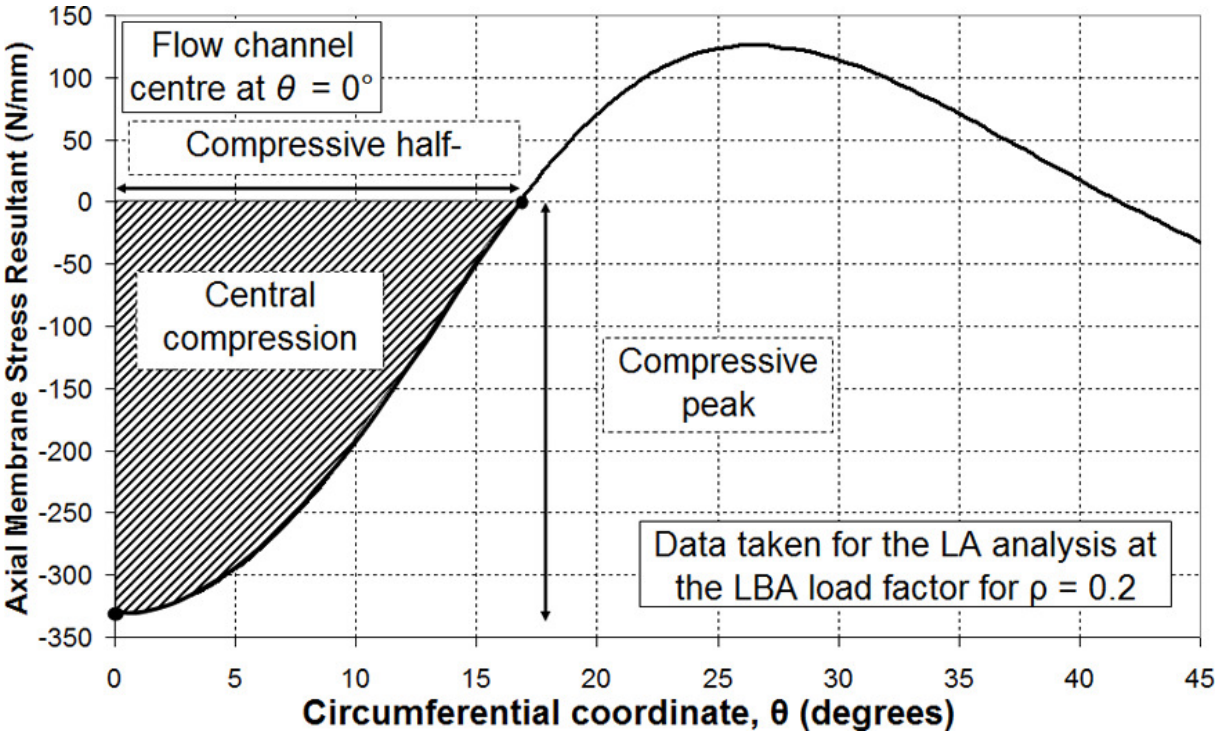


Fig. 16 - Illustration of the parameters of the axial membrane compression across the flow channel at the bottom of the 3 mm strake for a typical distribution

Published in: *ASCE Journal of Structural Engineering*, 138(7), 922-931.
DOI: http://dx.doi.org/10.1061/(ASCE)ST.1943-541X.0000530

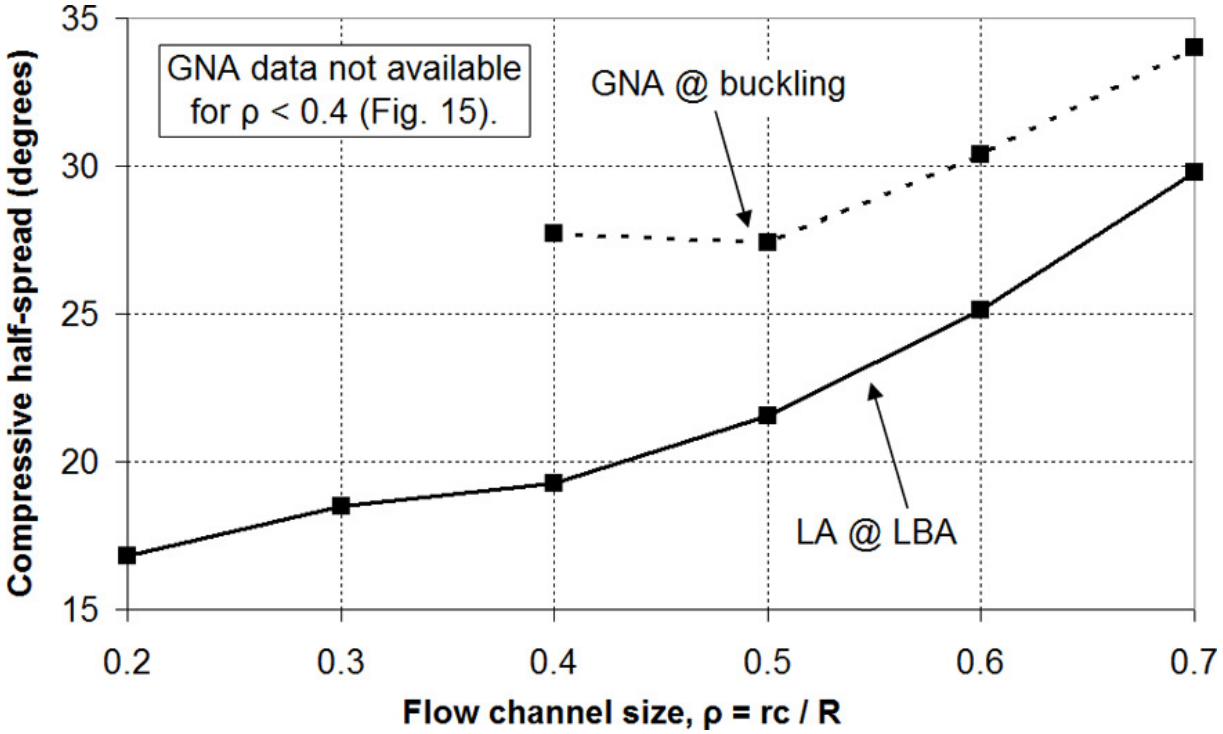


Fig. 17 – Variation of the half-spread of compressive axial membrane stress resultants at buckling through the bottom of the 3 mm strake

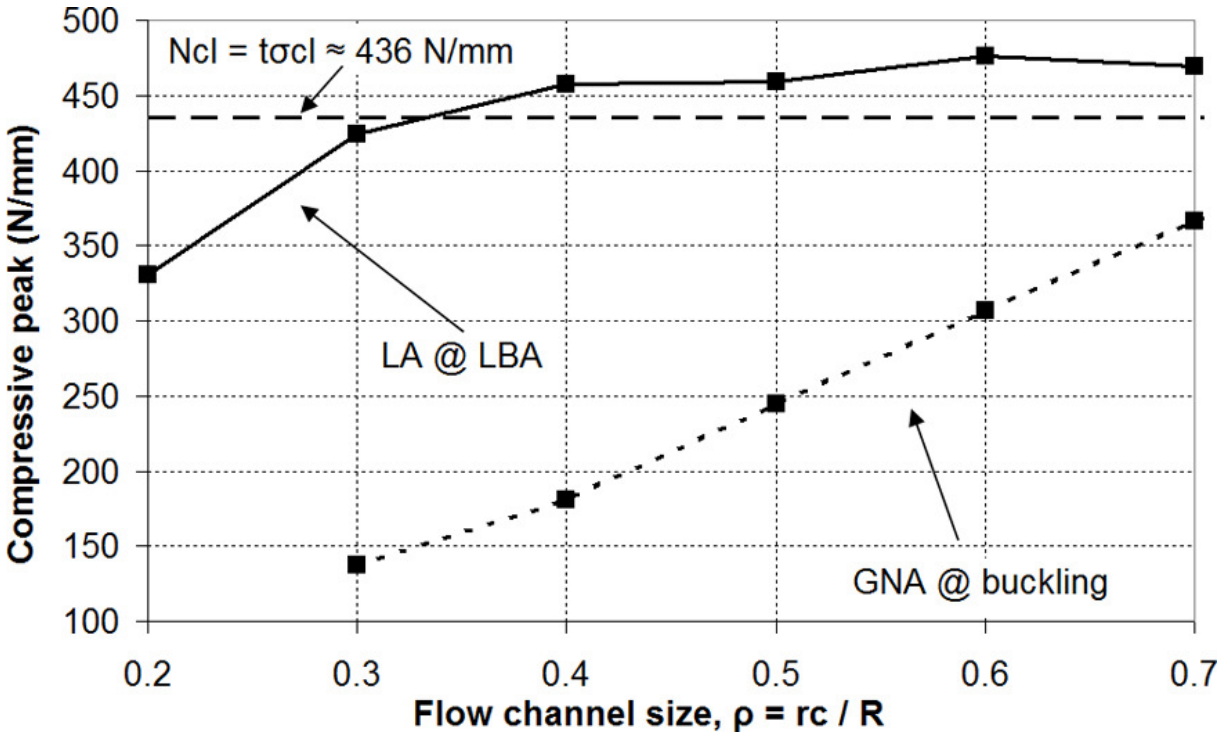


Fig. 18 – Variation of the peak compressive axial membrane stress resultant at the centre of the flow channel through the bottom of the 3 mm strake

Published in: *ASCE Journal of Structural Engineering*, 138(7), 922-931.
DOI: http://dx.doi.org/10.1061/(ASCE)ST.1943-541X.0000530

Behavior of the imperfect silo under eccentric pipe flow with different imperfection forms

This section investigates the effect of three different eigenmode-affine imperfection forms on the example silo under eccentric discharge: the inward 1st LBA mode, the outward 1st LBA mode and the deformed GNA shape just before buckling. The imperfection amplitudes were chosen as those prescribed in EN 1993-1-6 Annex D for hand-based design (Fig. 4) corresponding to the strake in which the peak magnitude of radial displacement occurs in the LBA analysis. In this study, this peak always lay within the thinnest 3 mm strake. The scaling procedure was similar for GNA pre-buckling modes, but the maximum absolute radial displacement from each GNA analysis at the increment just before buckling was first factored to unity, before being factored again to the required imperfection amplitude of the strake in which it occurred. Contrary to LBA analyses, the peak GNA pre-buckling displacement did *not* always occur within the 3 mm strake. The results of the elastic finite element analysis for the imperfect silo (GNIA) are shown in Fig. 19 as a function of the relative flow channel size ρ.

Table 2 – Load proportionality factors for the imperfect silo

$\rho = r_c/R$	0.00	0.10	0.20	0.25	0.30	0.40	0.50	0.60	0.70	0.80	0.90
GNA §	7.63	6.77	4.51	2.55	0.81	0.49	0.33	0.37	0.41	0.63	1.18
GNIA#1 †	3.40	6.15	4.58	3.43	2.04	2.55	1.31	1.59	0.17	0.25	0.66
GNIA#2 ‡	3.32	6.03	4.51	3.44	2.37	2.66	0.20	1.58	0.16	0.26	0.69
GNIA#3 *	5.21	4.33	5.93	6.98	3.03	3.43	0.80	0.49	0.41	0.59	0.94

§ - perfect shell; † - inward 1st LBA mode; ‡ - outward 1st LBA mode;
* - deformed GNA shape just before bifurcation

The first LBA buckling eigenmodes were previously shown in Fig. 10 and it is evident that their shape depends directly on the channel size ρ. The deformed shapes of silos at GNA buckling are similarly dependent on ρ. Eigenmode-affine imperfections modes are always related to the structure's geometry and loading conditions in a way that makes them most difficult to imagine in advance, unlike imperfections based directly on probable structural forms which may be expressed by a neat equation such as the axisymmetric weld depression of Rotter and Teng (1989).

Published in: *ASCE Journal of Structural Engineering*, 138(7), 922-931.
DOI: http://dx.doi.org/10.1061/(ASCE)ST.1943-541X.0000530

The shocking discovery from Fig. 19 is that the perfect shell buckling strength (GNA) is predominantly the *lowest* out of each of the three GNIA analyses. This figure shows that the effect of any one of these imperfection forms is strongly variable, and may result in either an increase or a decrease in the buckling strength in what appears to be an unpredictable manner. The reason for this is that each of the LBA buckling modes considered here consist of a series of tightly-spaced alternating inward and outward indentations in the silo wall at the bottom of the 3 mm strake, so it is not surprising that reversing these has little effect. Similarly, the GNA pre-buckling deformations consist of substantial indentations in the silo wall due to the high axial bending at the geometric discontinuity that is the change of plate thickness. These are then amplified further by the high axial compression (Brush and Almroth, 1976; Rotter, 1989), which are subsequently introduced as a part of the imperfection form in the GNIA analysis. It thus appears that this type of imperfection results in a beneficial stiffening effect against the substantial circumferential bending that occurs in the shell adjacent to the flow channel as a result of the pressure drop (Fig. 20). A similar phenomenon was found for the axisymmetric weld depression of Rotter and Teng (1989) and is documented in Sadowski and Rotter (2011c).

Published in: *ASCE Journal of Structural Engineering*, 138(7), 922-931.
DOI: http://dx.doi.org/10.1061/(ASCE)ST.1943-541X.0000530

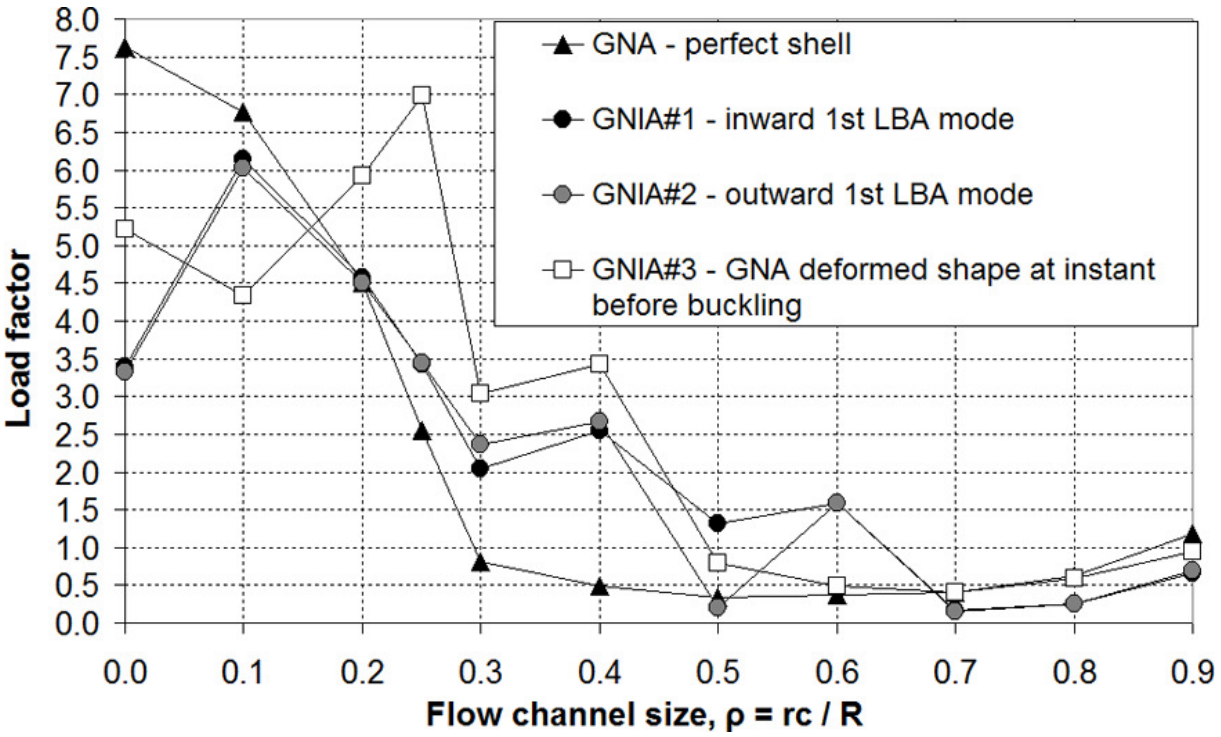


Fig. 19 – Variation of computed load proportionality factor for the imperfect silo with the relative flow channel size

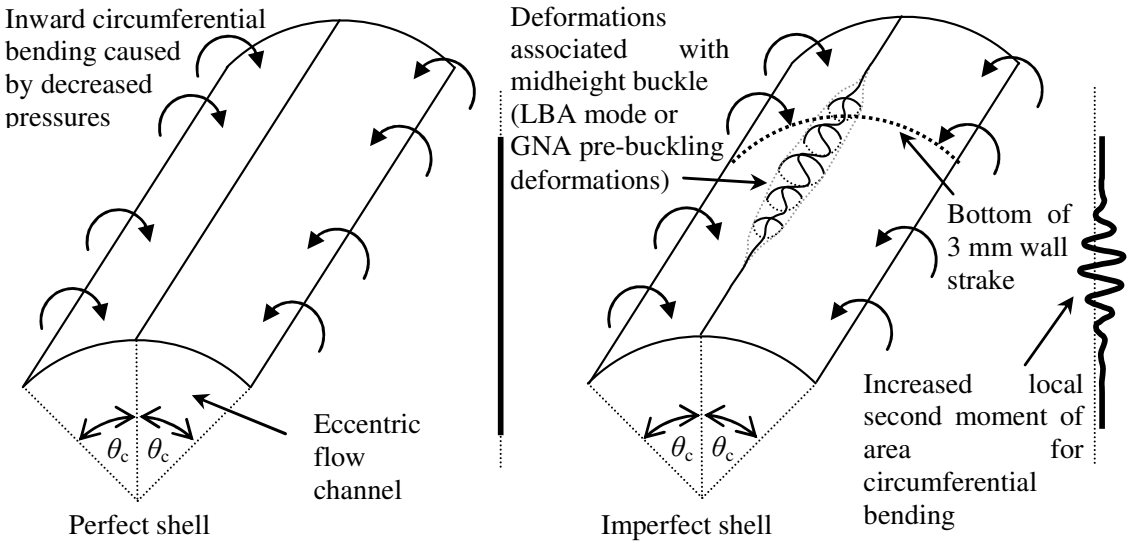


Fig. 20 – Comparison of the behaviour of the perfect and imperfect silo shells subject to eigenmode-affine imperfections

The eigenmode-affine imperfection forms thus have the unfortunate property that they produce a geometric form that is almost always systematically favourable. Given that the elastic 'midheight' buckling mode is a ubiquitous prediction for this load condition

Published in: *ASCE Journal of Structural Engineering*, 138(7), 922-931.
DOI: http://dx.doi.org/10.1061/(ASCE)ST.1943-541X.0000530

and is frequently observed in the field, this phenomenon will be seen in every LBA mode and GNA pre-buckling shape and there is no way to avoid this. Eigenmode-affine imperfections therefore cannot be relied upon to give strength decreases for silos under eccentric pipe flow discharge.

Conclusions

The following conclusions may be drawn on the basis of this study:

A slender thin-walled metal silo is very sensitive to the size of a flow channel under eccentric pipe flow discharge. The finite element predictions are also very different depending on whether the analysis is geometrically linear or nonlinear. Under realistic modelling conditions, the behavior of the silo is only very mildly affected by small flow channels, but very adversely affected by medium and large flow channels.

With geometric nonlinearity, a greater circumferential spread of the silo wall is mobilised to carry a greater portion of the compressive stresses which develop across the channel during eccentric discharge. This in turn reduces the peak compression and leads to significant gains in buckling strength.

Eigenmode-affine imperfection forms under eccentric pipe flow have been found to produce a geometric configuration that effectively stiffens the cylinder against circumferential bending and are thus beneficial to the buckling strength. These imperfection forms are not suitable for use in design for this load condition. A similar behavior was observed for the axisymmetric weld depression in previous studies.

It must be concluded that this structure is either insensitive to imperfections under eccentric pipe flow, or that a more exotic imperfection form remains to be found that may produce significant sensitivity and an adverse relationship between buckling strength and imperfection amplitude.

Published in: *ASCE Journal of Structural Engineering*, 138(7), 922-931.
DOI: http://dx.doi.org/10.1061/(ASCE)ST.1943-541X.0000530

References

ABAQUS (2009). "ABAQUS Version 6.9" *Dassault Systèmes Simulia Corp.*, Providence, RI, USA.

Brush D.O. & Almroth B.O. (1976). "Buckling of Bars, Plates and Shells." *McGraw-Hill*, New York.

Bucklin R.A., Thompson S.A. & Ross I.J. (1990). "Bin-wall failure caused by eccentric discharge of free-flowing grain." *Jrnl. of Struct. Eng.*, ASCE, 116(11), 3175-3189.

Cai M. (2003). "Buckling of cylindrical shells under non-uniform loads." *PhD Thesis*, The University of Edinburgh, UK.

Calladine C.R. (1983). "Theory of Shell Structures." *Cambridge University Press*, Cambridge.

Chen J.F. (1996). "Granular solid - structure interaction in silos." *PhD Thesis*, The University of Edinburgh, UK.

Chen J.F., Rotter J.M., Ooi J.Y., Zhong Z. (2007) "Correlation between the flow pattern and wall pressures in a full scale silo." *Engineering Structures*, 29, 2308-20.

EN 1991-4 (2006). "Eurocode 1: Actions on Structures, Part 4: Silos and Tanks." *European Committee for Normalisation,* Brussels.

EN 1993-1-6 (2007). "Eurocode 3: Design of Steel Structures, Part 1-6: Strength and Stability of Shell Structures." *Comité Européen de Normalisation*, Brussels.

EN 1993-4-1 (2007). "Eurocode 3: Design of Steel Structures, Part 4-1: Silos." *Comité Européen de Normalisation*, Brussels.

Esslinger M. & Geier B. (1972). "Gerechnete Nachbeulasten als untere Grenze der experimentellen axialen Beulasten von Kreiszylindern." *Der Stahlbau*, 41(12), 353-360.

Guggenberger W., Greiner R & Rotter J.M. (2004). "Cylindrical shells above local supports." Chapter 3 in *Buckling of Thin Metal Shells*, eds J.G. Teng & J.M. Rotter, Spon, London, pp 88-128.

Hampe E. (1987). "Silos, Band 1 - Grundlagen." *VEB Verlag für Bauwerke*, Berlin.

Jenike A.W. (1967). "Denting of circular bins with eccentric drawpoints." *J. Struct. Div.*, 93(ST1), 27-35.

Knödel P., Ummenhofer T. & Schulz U. (1995). "On the modelling of different types of imperfections in silo shells." *Thin-Walled Structures*, 23, 283-293.

Koiter W.T. (1945). "On the stability of elastic equilibrium." *PhD Thesis*, Delft University, Holland.

Koiter W.T. (1963). "The effect of axisymmetric imperfections on the buckling of cylindrical shells under axial compression." *Proc. Kon. Ned. Akad. Wet.*, B66, 265-279. (See also *Appl. Mech. Rev.*, 18, Review 3387, 1965).

Libai A. & Durban D. (1973). "A method for approximate stability analysis and its application to circular cylindrical shells under circumferentially-varying loads." *Jrnl. of Applied Mech*, Vol 40, Trans ASME, 971-976.

Libai A. & Durban D. (1977). "Buckling of cylindrical shells subjected to non-uniform axial loads." *Jrnl. of Applied Mech*, Vol 44, Trans ASME, 714-720.

Nielsen J. (1998). "Pressures from flowing granular solids in silos." *Phil. Trans. Royal Society of London: Philosophical Transactions: Mathematical, Physical and Engineering Sciences*, 1998, Series A, 356, 2667-2684.

Ooi J.Y., Pham L. & Rotter J.M. (1990). "Systematic and random features of measured pressures on full-scale silos." *Engineering Structures*, 12(2), 74-87.

Roberts A.W. & Ooms M. (1983). "Wall loads in large metal and concrete silos and silos due to eccentric draw-down and other factors." *Proc. 2nd Int. Conf. on Design of Silos for Strength and Flow*, Powder Advisory Centre, London.

Rotter J.M. (1985). "Design under axial compression." *Design of Steel Bins for the Storage of Bulk Solids*, ed. J.M. Rotter, The University of Sydney, Australia, 122-137.

Rotter J.M. (1986). "The analysis of steel bins subject to eccentric discharge." *Proc. of the 2nd Int. Conf. on Bulk Materials Storage, Handling and Transportation,* IEAustralia, Wollongong, 264-271.

Rotter J.M. (1989). "Stress Amplification in Unstiffened Cylindrical Steel Silos and Tanks." *Civil Eng. Transactions*, IE Aust, CE31(3), 142-148.

Rotter J.M. (2001). "Guide for the economic design of circular metal silos." *Spon Press*.

Rotter J.M. (2004). "Buckling of cylindrical shells under axial compression." Chapters 1 & 2 in *Buckling of Thin Metal Shells*, Eds J.G. Teng & J.M. Rotter, Spon, London, pp 1-87.

Rotter J.M. & Teng J.G. (1989). "Elastic stability of cylindrical shells with weld depressions." *Jrnl. of Struct. Eng.*, ASCE, 115(5), 1244-1263.

Rotter J.M. & Zhang Q. (1990). "Elastic buckling of imperfect cylinders containing granular solids." *Jrnl. of Struct. Eng.*, ASCE, 116(8), 2253-2271.

Rotter J.M., Cai M. & Holst J.M.F.G. (2011). "Buckling of thin cylindrical shells under locally elevated axial compression stresses." *Journal of Pressure Vessel Technology*, 133(1), 011204-1 to 11.

Sadowski A.J. & Rotter J.M. (2010). "A Study of Buckling in Steel Silos under Eccentric Discharge Flows of Stored Solids." *Jrnl. of Eng. Mech.*, ASCE, 136(6), 769-776.

Sadowski A.J. & Rotter J.M. (2011a). "Buckling of very slender metal silos under eccentric discharge." *Engineering Structures*, 33(4), 1187-1194.

Sadowski A.J. & Rotter J.M. (2011b). "Steel silos with different aspect ratios: I - behavior under concentric discharge." *Journal of Constructional Steel Research*, 67(10), 1537-1544.

Sadowski A.J. & Rotter J.M. (2011c). "Steel silos with different aspect ratios: II - behavior under eccentric discharge." *Journal of Constructional Steel Research*, 67(10), 1545-1553.

Song C.Y., Teng J.G. & Rotter J.M. (2004). "Imperfection sensitivity of thin elastic cylindrical shells subject to partial axial compression." *Int. Jrnl. of Solids and Structures*, 41, 7155-7180.

Teng J.G. & Song C.Y. (2001). "Numerical models for nonlinear analysis of elastic shells with eigenmode-affine imperfections." *Int. Jrnl. of Solids and Structures.*, 38(18), 3263-3280.

Yamaki N. (1984). "Elastic Stability of Circular Cylindrical Shells." *North-Holland*, Amsterdam.